JOURNAL OF GEOPHYSICAL RESEARCH, VOL. 88, NO. B7, PAGES 5806-5814, JULY 10, 1983

IMPACT EXPERIMENTS ON ICE

Shin-ichi Kawakami, Hitoshi Mizutani, Yasuhiko Takagi, Manabu Kato, and Mineo Kumazawa

Department of Earth Sciences, Nagoya University, Nagoya, 464, Japan

Abstract. The results of cratering and fragmentation experiments on pure ice are reported. The projectiles used are cylindrical aluminum, poly-carbonate, teflon, and pyrophyllite fired at velocities between 110 m/sec and 680 m/sec, with kinetic energies at impact between 2 and 500 joules. Crater diameters (pit diameters) in the ice were about two times larger than craters in the same energy range in basalts. The ratios of (pit diameter)/(spall diameter) are about three and the ratios of (depth of crater)/(spall diameter) are between 0.1 and 0.3 which are close to the depth/diameter ratios observed in basalts. The crater diameter in ice is also well expressed as a single function of the 'late-stage effective energy' defined recently by Mizutani et al. [1983]. The specific energy for complete destruction of ice target is about 50 J/kg which is two orders of magnitude smaller than that of basalt. The present experimental data on cratering and fragmentation of ice show that the impacts associated with the largest craters on Callisto and Mimas must have severely fractured the whole satellites, and that those giant impacts with the kinetic energy of 10^{23} to 10^{27} joules probably affected significantly the evolution of the satellites.

Introduction

Impact cratering and impact fragmentation are recognized as important processes in planetary accretion and in shaping the solid surfaces of planets and satellites in the solar system. Especially, recent Voyager I and II pictures of the icy Jovian and Saturnian satellites [e.g., Smith et al., 1979, 1981] suggest that comparison of cratering in icy targets with the extensively studied cratering data in silicate targets is important. Is the crater diameter versus kinetic energy relation for icy targets the same as that obtained for silicate targets? Is the crater morphology on ice similar to those observed on silicate targets and can we deduce some information on projectiles from crater morphology?

The presence of very large craters on Mimas, Ganymede, and Callisto indicates that very heavy collisions occurred on these icy satellites sometime in their histories. How could they survive the heavy collisions without disruption and grow to the present size?

The present study aims to provide basic data to answer these questions. We report results on cratering experiments and fragmentation experiments on pure ice and compare the results with those on rocky materials.

Earlier studies on the impact experiments on pure ice [Croft et al., 1979; Lange and Ahrens, 1981] are limited in the projectile velocity range and its kinetic energy range. In the present study, we perform the experiments in the velocity range from 110 m/sec to 680 m/sec, and in the kinetic energy range from 2 to 500 joules, so that we can better understand the cratering process or fragmentation process in a wider experimental condition than earlier studies by combining the present data with the results of the earlier studies. Recently, Lange and Ahrens [1982a,b] independently made impact experiments similar to the present study, extending the impact conditions of their earlier study [Lange and Ahrens, 1981] to those comparable to the present study.

Paper number 2B1775.
0148-0227/83/002B-1775$05.00

Experimental Procedure

The cratering experiments were performed on commercially sold rectangular ice blocks ($28\times28\times34$ cm^3 in size). We cut all edges and corners by a plane in order to lessen the effects of spallation at the corners and edges of the ice blocks. The commercial method of freezing produced a bloom-shaped zone consisting of numerous minute cylindrical pores in the center of a matrix which consists of elongated rodlike crystals and pores oriented perpendicular to the axis of the bloom zone (a half of the zone is seen in Figure 1b). The longer axis of crystals in the matrix was confirmed to be coincident with the crystallographic c-axis of ice. All the shots presented in this paper are made on the surface whose normal is parallel to the longer axis (c-axis) of rodlike crystals.

Compressive yield strength of the ice block is measured at uniaxial static loading [Masuda et al., 1982]. In the temperature range in which the present experiments were done (i.e., T = 265 ±3° K), the strength along the axis, which parallels with the direction of impact loading is about 4.5 MPa, whereas the strength along the direction perpendicular to the above axis is only about 3.0 MPa. Therefore the ice blocks used in the present study are highly anisotropic and are not intended to simulate natural targets such as icy satellites. Even so the present data are useful to clarify the cratering process in pure ice with minimum effect of pores and cracks.

The ice targets were stored in a freezer at temperatures of about 263° K for a period long enough for the target to attain thermal equilibrium (longer than a day). Then the targets were quickly transferred on a polyurethane foam sheet 5 cm thick in the vacuum chamber. The polyulethane foam sheet was precooled at a temperature of about 260° K, before the target was set on it. Then we evacuated the vacuum chamber to a pressure less than 10 mmHg. Sublimation of the ice in the vacuum chamber helped to keep the surface temperature of the ice target below

TABLE 1. Projectiles Used in This Study

Material	Density g/cm³	Mass g	Diameter cm	Length cm
Aluminum (2017)	2.8	7.4	1.5	1.5
		2.2	1.0	1.0
		0.4	0.5	0.76
		0.2	0.5	0.38
Teflon	2.2	1.7	1.0	1.0
		0.3	0.5	0.76
Poly-carbonate	1.4	0.2	0.5	0.76
Pyrophyllite	2.7	2.1	1.0	1.0

270° K. The target was impacted within twenty minutes after it was set in the vacuum chamber. The temperatures measured by thermocouples at two different positions in the ice blocks indicate that the temperature of the target was maintained at a temperature of 265±3° K.

We used several materials as projectiles, as listed in Table 1. These are designed in order to see the effect of projectile material on cratering process in ice. All projectiles were fired by the vertical single stage powder gun at the Department of Earth Sciences, Nagoya University [Mizutani et al., 1981].

The fragmentation experiments were performed in exactly the same procedure as that described above, except that the sizes of the some targets were made smaller than the original block. The original block weighted about 26 kg and the smallest blocks used in the fragmentation experiments weighted 1.8 kg, so that we could cover the specific energy range (= kinetic energy per unit target mass) from 4.2 to 260 J/kg.

The ice blocks were set on a polyurethane foam sheet, 5 cm thick, to approximate the free surface condition at the bottom surface. The other five surfaces of the ice blocks than the bottom surface were, of cource, free surfaces.

Immediately after the impact, the cratered target or fragmented target was photographed and a number of fragments, if any, were picked up and put into separate cans which were later weighted to know the size distribution of fragments. The diameter and depth of the crater, lengths of representative radial cracks, and diameters of concentric spalling craters, if any, were measured for every experiment. For some experiments, we cut the targets to a half and observed patterns of cracks developed inside the target.

Cratering Experiments

Fracture Patterns

Morphology of a crater formed in ice is characterized by a bowl-shaped central pit, long radial cracks extending from the impact point and fine concentric fractures. Figure 1 shows an example: this is a crater formed by an aluminum projectile (m = 2.0 g) at impact velocity of 465 m/sec. Figure 1b is the cross section of Figure 1a, showing the subsurface fractures. It seems that there are three types of large cracks in existence. The first one is the type of a crack which appears as a long radial crack on a plane view as shown in Figure 1a, and whose fracture surface is normal to the upper surface of the sample, as shown on the right in Figure 1b. The second type of a crack starts at the bottom of a crater and extends more or less horizontally, showing an undulatory surface in the cross section (the crack which reaches at the upper right corner of the label in Figure 1b). Sublateral cracks branching from this type crack tend to extend toward the upper surface of the target, leading to concentric spall fractures. The third type of crack is a rather straight down-going crack from the bottom of a crater as shown in the center of Figure 1b. But this type of crack may represent grain-boundary fracture of tabular ice crystals and may not be a general characteristic of ice craters. Those fracture patterns observed in impacted ice targets resemble those found in rock targets [Hörz, 1969; Curran et al., 1977], and are exactly the same as those reported recently by Lange and Ahrens [1982a]. The fracture pattern observed here is also similar to those produced in a soda-lime glass by indentation experiments [Lawn and Wilshaw, 1975; Lawn and Swain, 1975]. The similarity of the fracture pattern between the two indicates that the mechanism of the indentation fracture may be applicable to the fractures

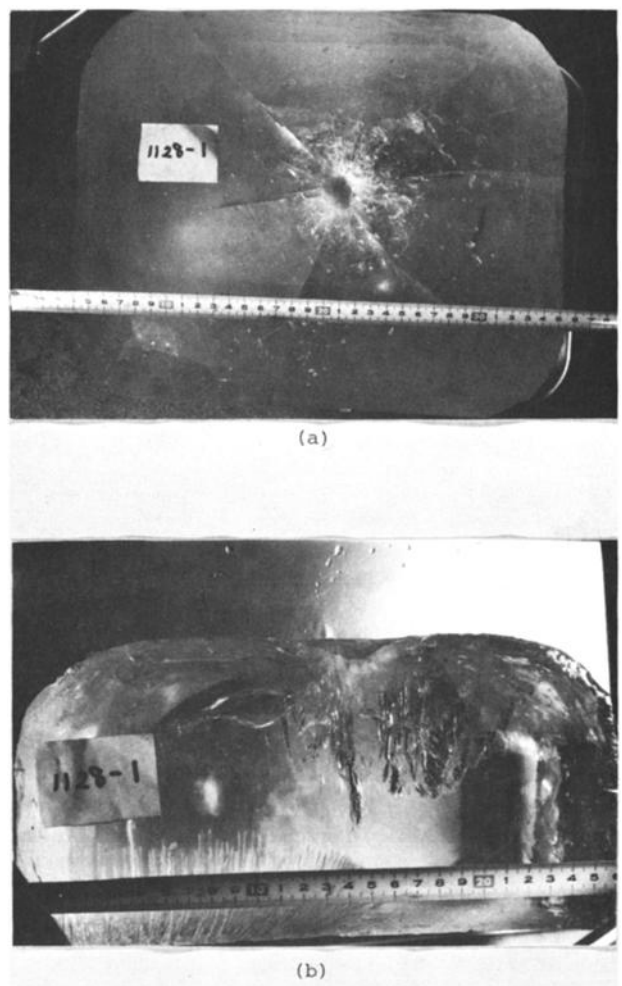

Fig. 1. A crater formed in ice. Aluminum projectile with m = 0.20 g was impacted in the ice block at velocity, v = 465 m/sec. (a) overhead view. (b) section profile beneath the crater.

TABLE 2. Experimental Data of Craters Formed in Ice

Run Number	Projectile Mass (g)	Velocity (m/s)	Kinetic Energy (J)	Spall Diameter (cm)	Pit Diameter (cm)	Depth (cm)	Comments
			Aluminum projectile				
1024-1	2.15	141	21.4		2.9	1.1	
1104-1	0.41	336	23.1		2.9	2.6	
1106-1	0.40	162	5.25	4.3	1.9	1.1	
1107-1	0.20	162	2.62		1.5	0.5	
1107-2	0.40	112	2.51		1.5	0.6	
1107-3	0.40	140	3.92	4.0	1.3	0.5	
1109-1	0.19	345	11.3	4.8	1.5	2.4	
1109-2	0.41	164	5.51		1.7	0.6	
1109-3	0.18	154	2.13	4.0	1.4	0.4	
1111-1	0.18	500	22.5	9.8	2.4	2.9	
1111-2	0.12	537	17.3	9.4	2.7	2.6	
1113-1	2.22	133	19.6	6.0	3.0	1.0	
1113-2	0.18	489	21.5	9.5	3.8	2.5	
1114-1	0.40	333	22.2	10.0	2.6	1.3	
1114-2	0.12	554	18.4	8.9	2.5	1.4	
1117-1	2.22	130	18.8	6.4		1.0	
1117-2	0.40	349	24.4	7.6	3.0	1.8	
1128-1	0.20	465	21.6	8.6	3.1	1.6	
1128-2	0.12	533	17.0	12.5	2.1	2.1	
1209-1	0.40	140	3.92	4.0	1.4	0.7	
			Teflon projectile				
1203-1	1.71	214	39.2	9.7		1.1	block splitted
1205-3	1.71	159	21.6		2.0	0.9	tabular plateau
1205-4	1.69	148	18.5	4.8	2.3		
1208-4	0.32	159	4.04		3.9	0.3	tabular plateau
1208-5	0.32	129	2.66		3.9		
1209-1	0.31	140	3.04	3.3	1.3	0.4	
1209-2	1.68	130	14.2	5.8	2.4		tabular plateau
1212-1	1.69	141	16.8	4.5	2.4		tabular plateau
1212-2	0.30	237	8.43	3.1	2.0	0.7	tabular plateau
1217-1	1.66	185	28.4	8.0	2.4	1.0	tabular plateau
1217-2	0.31	186	5.36	4.3	2.1		tabular plateau
			Poly-carbonate projectile				
1211-1	0.21	148	2.30	2.5	1.2	0.4	
1211-2	0.20	152	2.31	3.4	1.3	0.4	
1211-3	0.21	321	10.8	6.5	2.6	0.8	
1211-4	0.21	292	8.95	9.5	1.7		
1211-5	0.20	350	12.3	8.3	2.3	1.0	tabular plateau
			Pyrophyllite projectile				
20108-1	2.10	180	34.0	6.5	3.3	1.3	
20108-2	2.13	151	24.3	6.5	3.3	1.3	

produced by the low velocity impact experiments. The shape of central pits produced by teflon or poly-carbonate projectiles' impacts show sometimes tabular plateaus in the center of the pits, as schematically shown in the inset of Figure 5. This is similar to the central peaks observed in quartz sand craters produced by 15ϕ aluminum projectiles at velocities of 300 to 400 m/sec [Mizutani et al., 1983]. Since the relation of the tabular plateau seems to be highly compressed by a plane shock wave and to be produced only by a cylindrical projectile, this feature may be a remnant of the highly shocked central zone, in which the target material is so well compressed that it could survive fracturing stress at a late stage.

Crater Diameter Versus Kinetic Energy Relation

Table 2 summarizes impact condition and crater size for the thirty-eight impact experiments. Figure 2 is a diagram showing the variation of diameter of craters produced by impact of aluminum projectiles with kinetic energy. In this figure, the data by Croft et al. [1979] for pure ice are added to ours and the D-E relation for basalt obtained by Gault [1973] is also shown for comparison. The solid symbols are the data for pit diameters and the open symbols are for spall diameters which are defined by the largest and most notable concentric spall cracks. The data denoted by triangles are the data obtained additionally by H. Mizutani using some rifle guns at less-controlled experimental conditions (the experiments were television broadcasted for a popular science program in 1979). Those experimental data are separately listed in Table 3. Figure 3 shows the similar data obtained by projectiles of teflon, poly-carbonate, and pyrophyllite. All the data points for pit diameters shown in Figure 2 and 3 fall around a single line parallel to the line for basalts obtained by Gault [1973]. Assuming the

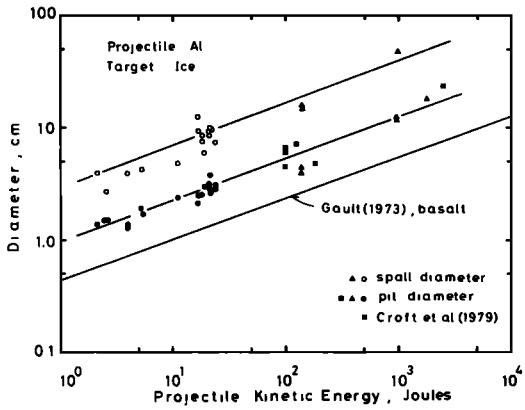

Fig. 2. Dependence of diameter on the projectile kinetic energy for craters formed in ice by aluminum projectiles. The data shown by black squares are those reported by Croft et al. [1979]. The data shown by triangles are those obtained by firing bullets with rifles.

slope of the line the same as that for basalts, we obtain the following relations of the pit diameter, D_p versus the kinetic energy, E and the spall diameter, D_s versus E for craters in pure ice:

$$D_p(m) = 0.95\times10^{-2}\ E(J)^{0.37} \quad (1)$$

$$D_s(m) = 2.85\times10^{-2}\ E(J)^{0.37} \quad (2)$$

These relations agree well with the relation proposed by Croft et al. [1979],

$$D_p(m) = 0.883\times10^{-2}\ E(J)^{0.4} \quad (3)$$

and comparable with the recent results by Lange and Ahrens [1982a]

$$D_s(m) = 1.7\times10^{-2}\ E(J)^{0.31} \text{ at } T = 257^\circ\ K \quad (4)$$

$$D_s(m) = 1.48\times10^{-2}\ E(J)^{0.32} \text{ at } T = 81^\circ\ K \quad (5)$$

The present equation (2) is more close to (4) obtained at T = 257° K than (5) at T = 81° K. The difference between (2) and (4) may indicate our ice samples at T = 265±3° K had a smaller apparent strength than Lange and Ahrens's samples at T = 257° K. But the overall agreements among the data sets obtained at different laboratories are satisfactory, considering rather different procedures of ice sample preparation.

The spall diameters of craters produced by aluminum projectiles seem consistently a little larger than those produced by teflon projectiles, but its significance is not yet clear because the scatter of data points is rather large in the case of the spall diameters. If we use the data obtained by aluminum projectiles, the spall diameter is about three times larger than the pit diameter:

$$D_s/D_p = 3.0 \quad (6)$$

The ratio of (spall diameter)/(pit diameter) found here on ice is smaller than the average ratio (D_s/D_p = 4.5) found in micrometeorite craters on lunar rocks [Hörz et al., 1971]. The difference may be either due to the difference in target material or due to the difference of impact velocity, or due to the difference of crater size (the present data = 1 ∿ 10 cm; microcrater = 10 ∿ 100 μm). Further research on this difference is required.

Equation (1) shows the pit diameter in ice is about twice as large as craters in basalt for a given impact, because Gault's [1973] equation for basalt is

$$D(m) = 0.428\times10^{-2}\ E(J)^{0.37} \quad (7)$$

The difference between (1) for ice and (7) for basalt may be due to the difference of strengths between the two target materials.

Recently Mizutani et al. [1983] suggested that the parameter named as the 'late-stage effective energy', I, is more important to describe cratering process than impact kinetic energy. Therefore we plotted the present data on the pit diameter as a function ot the late-stage effective energy in Figure 4. The data are best fit within the following equation:

$$D = k\{\tfrac{1}{2}\, m(C_o + \tfrac{1}{2}\, sv)v\}^{2/5} \quad (8)$$

where k is a constant and is determined by the D-I relation in Figure 4 to be 4.0×10^{-3} m $J^{-5/2}$, m is projectile mass, C_o and s are parameters relating the shock-wave velocity, U, to the particle velocity, u, in the following empirical equation: $U = C_o + su$. Here we used the values of G. D. Anderson [1967] cited in Kieffer and Simonds [1980] for C_o and s of ice:

$$C_o = 1.28 \text{ km/sec} \quad (9)$$

$$s = 1.56$$

The form of (8) is the one suggested by Mizutani et al. [1983], for strength dominated cratering. The good agreement of the theoretical prediction with the experimental data supports the usefulness of Mizutani et al.'s scaling. Later in the present study, we will use the scaling law to apply the present experimental data to the planetary cratering.

In Figure 5, we showed variation of depth of craters with spall diameters. As shown in the inset of the figure, deep central pits are produced in craters produced by high density

TABLE 3. Results of Impact Experiments on Ice Obtained by Firing Bullets With Rifles

Run Number	Bullet Type	Velocity (m/sec) initial	final	Projectile mass (g)	Energy (J)	D_p (cm)	D_s (cm)	Depth (cm)
#1	22 long	380	330	2.6	142	4	∿15	∿7
#2	22 long	380	330	2.6	142	4.5	∿16	
#3	Carbin	600	530	7.1	997	12	∿48	16
#4	Carbin	600	530	7.1	997	12	∿48	16
#5	Slag#12	490	370	26	1780	19		∿20

projectiles (aluminum and pyrophyllite), and tabular plateaus are formed in craters produced by low density projectiles (teflon and poly-carbonate). Therefore the depth/diameter ratio is generally larger for a crater produced by a high density projectile than that produced by a low density projectile. Earlier studies [Gault, 1973; Croft, 1981; Summers and Charters, 1959] suggested that the depth of a crater is a primary function of (ρ_p/ρ_t). Since the data obtained in this study are highly scattered, we can not obtain clear functional form of the depth versus (ρ_p/ρ_t) relation, but the overall-trend of the present data is consistent with the empirical relation proposed by Croft [1981]. The average value of the depth-diameter ratios of ice craters is, however, between 0.1 and 0.3 which is close to the depth-diameter ratios observed in basalt [Gault, 1973]. This observation of the depth-diameter ratios is contradictory with the observations by Croft et al. [1979] who stated the depth-diameter ratios of craters in ice are nearly 0.5, but in good agreement with recent studies by Lange and Ahrens [1982a]. Since the data of Croft et al. [1979] were for craters produced by firing ordinary gun bullets, their larger depth-diameter ratios might be due to spin of the bullets and/or due to the high density of the projectiles. Our experiments using the standard rifle gun also produced craters with larger depth-diameter ratios such as obtained by Croft et al. [1979].

Fragmentation Experiments

Fragmentation Energy

The mode of impact fragmentation of solids varies with increase in the projectile kinetic energy per unit target mass [Fujiwara et al., 1977]. Earlier studies on the impact fragmentation of silica glass, basalt, and water ice revealed that specific energies (projectile energy/target mass) required for catastrophic destruction are 10^3, 6×10^3, and 30 J/kg respectively [Gault and Wedekind, 1969; Fujiwara et al., 1977; Hartmann, 1978]. Table 4 summarizes impact conditions and the results of impact for present experiments. Figure 6 shows the relation between the ratio of the maximum fragment mass

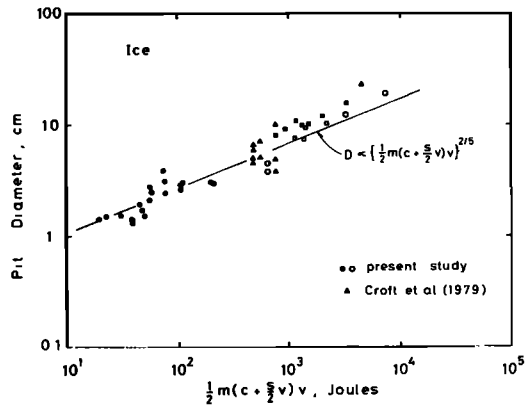

Fig. 4. Dependence of pit diameter in ice on the late-stage effective energy.

normalized by the original target mass and the specific energy for each impact. The data obtained for other rocky materials [Kawakami, 1982] and Fujiwara et al's [1977] relation for basalt are also shown for comparison. In specific energy below 2 J/kg, we observe only cratering in ice. Splitting of a target ice block to a few large blocks was observed at impacts with specific energy at around 3 J/kg. The core type fragmentation observed for basalts [Fujiwara et al., 1977; fragmentation class II in the terminology by Lange and Ahrens, 1981] was not observed for ice in the present study. Figure 6 indicates that the M_{max}/M_{target} (maximum fragment mass/target mass) versus specific energy (kinetic energy/target mass) relations of various materials take a very similar form in this diagram, though the scatter of the data points is large. The specific energy required for complete destruction ($M_{max}/M_{target} \sim 5 \times 10^{-2}$) of ice is about 50 J/kg which is two orders of magnitude smaller than that for basalts. The present data are in better agreement with the data at T = 81° K by Lange and Ahrens [1981] than the data at T = 257° K by the same authors. This is inconsistent with comparison of cratering experiments indicating that our ice samples at T = 265±3° K are more similar in mechanical properties to Lange and Ahrens' samples at T = 257° K than to their samples at T = 81° K.

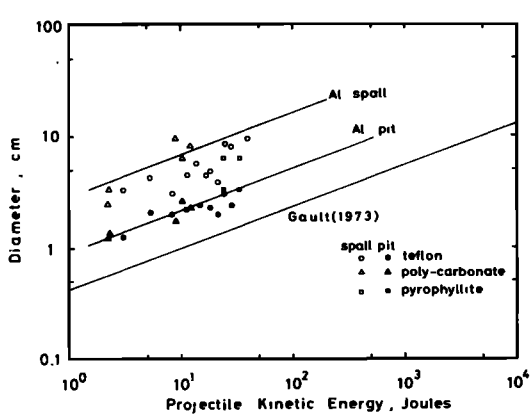

Fig. 3. Dependence of diameter on the projectile kinetic energy for craters formed in ice by using teflon, poly-carbonate and pyrophyllite as projectiles.

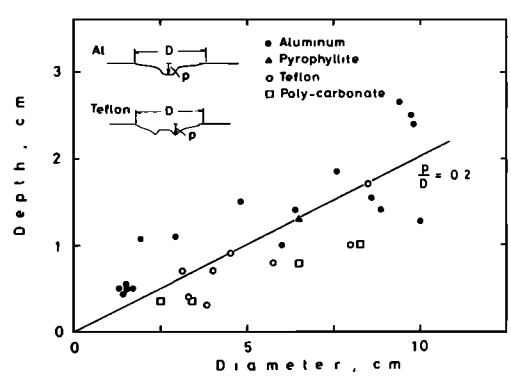

Fig. 5. Relation between the depth and the diameter of craters formed in ice. The depth/diameter ratio is about 0.2 for ice as shown by the straight line in the figure. The depth/diameter ratio seems to increase as the projectile density increases.

TABLE 4. Experimental Data of Fragmentation of Ice

Run Number	Projectile Mass (g)	Velocity (m/sec)	Kinetic Energy (J)	E_k/M_{target} (J/kg)	M_{max}/M_{target}
1022 - 1	2.23	680	516	20	0.16
1024 - 1	2.15	141	21.4	2.1	>0.99
1028 - 1	2.15	279	83.7	5.7	0.30
1029 - 1	2.21	142	22.3	4.2	0.44
1029 - 2	2.22	141	22.1	12	0.58
1104 - 1	0.41	336	23.1	1.7	>0.99
1104 - 2	2.22	500	278	260	0.02
1105 - 1	2.16	525	298	47	0.07
1106 - 2	2.21	143	22.6	4.3	0.38

According to Lange and Ahrens' experimental results, larger craters are produced and higher energies for destruction are required in ices at T = 257° K than in ices at 81° K. But the present experiments show that in our ice samples larger craters are produced and smaller energies for destruction are required than in Lange and Ahrens' samples at T = 81° K. The discrepancy between the two results suggests that cratering process does not reflect the same mechanical property as that involved in the fragmentation process: cratering may be controlled by the strength which is the maximum stress that the material can support and fragmentation may be controlled by the fracture energy, which is the energy required to make a new fracture surface. The ice samples in the present experiments may have lower strengths and lower fracture energies than those used by Lange and Ahrens [1981, 1982b]. The two orders of magnitude difference of the specific energy between ice and basalt may, however, be related to the differences of their strengths, because the static compressive strength of the ice is also about two orders of magnitude smaller than that of basalt. Probably the strength relevant to fracturing by impact process, i.e., strength at high strain rate, maintained approximately the ratio observed for the static compressive strength: experimental data on the strain-rate dependence of strength of ice [Hobbs, 1974] is also 1.5 to 2.0 orders of magnitude smaller than those of silicate rocks [Mizutani and Spetzler, 1983]. A full discussion on the specific energy versus material strength relation will be given in a future paper [Mizutani et al., in preparation]. An implication of Figure 6 is that the specific energy characterizing the fracture mode may be proportional to the compressive failure strength of the target material. The low specific energy of ice required for fragmentation indicates that accretion of icy bodies may be much more difficult than accretion of rocky or metallic bodies, if other things are the same [Greenberg et al., 1978; Matsui, 1979]. But this inference must be tested after the velocity distribution of fragments produced at impacts is firmly established.

Size Distribution of Fragments

Fragments of ice were quickly recovered after the impact experiments and put into separate cans. These are later weighted and the weight of each fragment is then determined subtracting the weight of the can from the total weight. We could only count fragments larger than a few grams, because the number of smaller fragments became too large to handle and smaller fragments melted at room temperature too rapidly to be weighted precisely. The shape of each fragment was not measured as Fujiwara et al. [1978] and Lange and Ahrens [1981] did, because our target was very anisotropic and the fragmental shape tended to be columnar, reflecting the original grain texture of the target. This feature may be related to the fact that our experiments did not show the core-type fragmentation as observed by Fujiwara et al. [1977] and Lange and Ahrens [1981]. Figure 7 shows the size distribution of fragments, in which the cumulative number of fragments larger than a mass m is plotted. Although the cumulative number versus m/M_{max} curves seem rather erratic, the curves showing the size distributions of fragments produced at impacts with the specific energies larger than 50 J/kg are of the similar slope in the range of N > 15. The curves in this range are approximately expressed by

$$N = C\, m^{-2/3} \qquad (10)$$

where N is the cumulative number of fragments heavier than m, and C is a constant. Equation (10) is identical with the well-known Gaudin-Schumann relation in comminution engineering

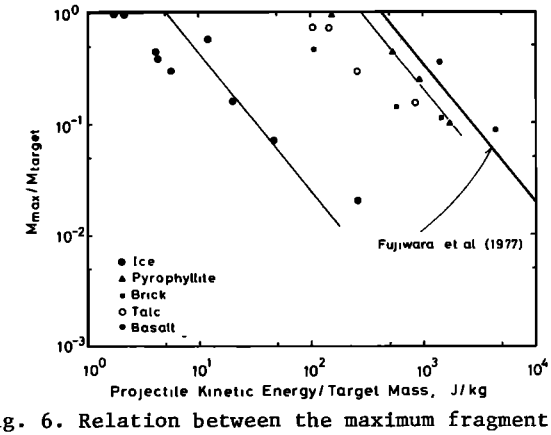

Fig. 6. Relation between the maximum fragment mass normalized by the original target mass and specific kinetic energy. The thin lines are eyeball fits to the data on ices and on pyrophyllite. The slopes of the lines are fixed to be the same as the Fujiwara et al.'s [1977] relation for basalts.

[Takeuchi and Mizutani, 1964; Schumann, 1940]. When the specific energies are smaller than 5 J/kg, the number of fragments in the mass range of $m/M_{max} = 10^{-2}$ to 10^{-3} ($m \sim 20$ grams) is extremely small. Figure 7 indicates that there may be two regions in the N versus m/M_{target} curves: the regime I in which N is smaller than 15, and slopes of the curves may increase with the specific energy, and the regime II, in which the curves are approximated by (10). The size distribution of impact fragments of pyrophyllite, shown in Figure 8, suggests more clearly the existence of the two regimes in the size distribution of impact fragments. The size distribution of basalt fragments obtained by Fujiwara et al. [1977] is not inconsistent with the above observation, though their data show more erratic nature of the size distribution than those on pyrophyllite. Lange and Ahrens [1981] observed that the size distribution of ice fragments from all fragmentation classes were a strong function of the specific kinetic energy of the projectile. Considering their specific energies are larger than 10 J/kg, their observations are related to the present observation in regime I and consistent with the present results. If this observation holds universally for size distribution of any impact fragments, it may give a significant influence on the accretion and/or fragmentation processes in the early solar system. A more detailed study on the size distribution of impact fragments, especially in the regime I, will be made in our forthcoming papers.

Discussion

Recent Voyager I and II pictures of the icy Jovian and Saturnian satellites show that there are many impact craters on these satellites [Smith et al., 1979, 1981]. Especially, the Saturnian satellite Mimas has an impact crater larger than one-quarter the diameter of the satellite. The Jovian satellite Callisto also has large impact craters; the central bright spot of the largest crater, Valhalla is about 600 km across, and its concentric rings extend outward about 1500 km from the impact center. In the present section, we would like to discuss implications of these gigantic impacts, using the present experimental data.

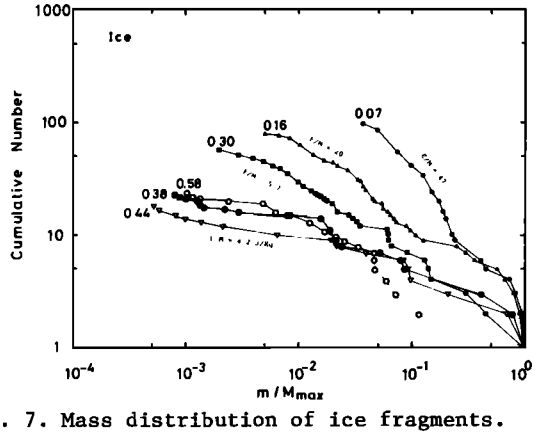

Fig. 7. Mass distribution of ice fragments. The fragment mass normalized by the maximum fragment mass is selected for the horizontal coordinate. The value attached to the left end of each curve is the ratio M_{max}/M_{target} for each impact.

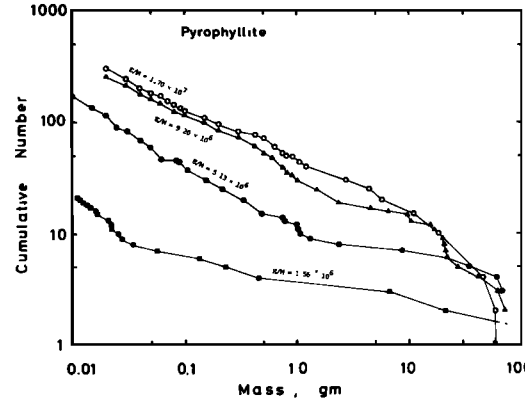

Fig. 8. Mass distribution of pyrophyllite fragments produced by the impact of aluminum projectile.

According to Mizutani et al's [1983] general scaling relationship, the crater diameter in ice in the strength-dominated regime is expressed by (8):

$$I = K D^{3/2} \tag{11}$$

where

$I = m(C_o + sv/2)v/2$
D = diameter,
K = constant.

The constant K is directly connected to the constant k in (8):

$$K = k^{-3/2} \tag{12}$$

When the diameter of a crater becomes large enough and its gravitational energy to lift ejecta material becomes larger than the energy consumed to fracture the target material, (i.e., in the gravitational-scaling regime), we should have a different relationship between D and I. Mizutani et al's [1983] general scaling relationship suggests the following equation:

$$I = K_1 D^4 + K_2 D^{3/2} \tag{13}$$

where K_1 is a constant proportional to the gravitational acceleration, g. The constant K_1 is obtained from the experimental data on noncohesive (i.e., $K_2 = 0$) targets. Using the data of impact cratering in quartz sand [Mizutani et al., 1982], we estimate K_1 on a planet with the gravitational acceleration, g, as follows:

$$K_1 = K_1' (\rho g/\rho_o g_o)$$
$$= 6.82\times10^5 (\rho g/\rho_o g_o) \quad (J/m^4) \tag{14}$$

where $g_o = 9.80$ m/sec^2, ρ_o = density of quartz sand (= 1590 kg/m^3), ρ = density of a planet, g = gravitational acceleration on a planet. The constant K_1' was obtained from the Mizutani et al's [1983] data on craters formed in sand (see their Figure 10). The constant K_2 is obtained from the present experimental data by (11), (the value is given by (12) and k in (8)),

$$K_2 = 9.88\times10^5 \quad (J/m^{-3/2}) \tag{15}$$

TABLE 5. Physical Parameters Used in the Present Calculation

	Mimas	Callisto
Mass (10^{20} kg)	0.3725	1063
Radius (km)	195	2420
Mean density (kg/m^3)	1200	1790
Gravity (m/sec^2)	0.0653	1.21
Bulk sound velocity (km/sec)	1.28	1.28
$s = \{(\partial K/\partial p) + 1\}/4$	1.56	1.56

The above constant K_2, however, is for the pit diameter, D_p, and the corresponding constant, $K_{2,s}$, for the spall diameter, D_s, is obtained as follows by noting $D_s/D_p = 3.0$:

$$K_{2,s} = 6.34\times10^4 \quad (J/m^{-5/2}) \qquad (16)$$

The above constant K_2 was derived from the experimental data obtained at T = 265° K. The constant may change with decreasing temperature because strength of ice is known to increase with decreasing temperature [Butkovich, 1959; Lange and Ahrens, 1982a]. According to Lange and Ahrens [1982a], the peak compressive strength of H_2O ice is about 1.5 times as large as that at T = 257° K. Since the constant K_2 is thought to be linearly proportional to the strength [Gault and Wedekind, 1977] and the difference of a factor of 1.5 in the K_2 is within the uncertainty of analyses, we ignore the change of K_2 with temperature at present.

Using (13), (14), and (15) with appropriate values for g, ρ, C_0, and s which are listed in Table 5, we can calculate the relation between impact crater diameter and kinetic energy of projectile. In Figure 9 the results for Callisto and Mimas are shown. Although the application of the experimental cratering data to these satellites requires extrapolation of five to seven orders of magnitude in diameter and 20-25 orders of magnitude in kinetic energy, we believe the way of extrapolation is much more reliable than the simple extrapolations of experimental D-E relations such as done by many previous workers. Particularly the present extrapolation is superior to other previous ones in utilizing the late-stage effective energy as a major parameter characterizing an impact process. As discussed by Mizutani et al. [1983], use of the late-stage effective energy leads to a more general scaling which seems to be valid in a wide range of impact conditions. Since the present theoretical D-E relation depends on the projectile mass in the momentum controlling regime [Mizutani et al., 1983], two cases for m = 1 gram and 10^6 grams are shown to illustrate the dependence of the projectile mass. But the dependence of the projectile mass on the D-E relation disappears in both satellites at $D > 10^2$ m: in the region $D > 10^2$ m, we obtain the ordinary gravity scaling relationship for both satellites. Because Mimas' surface gravity (0.0653 m/sec^2) is about 1/20 of the Callisto's surface gravity (1.21 m/sec^2), the diameter of a crater on Mimas is 2.1 (= $20^{1/4}$) times larger than that of a crater on Callisto, produced at impact with a same kinetic energy. Here we used the relation

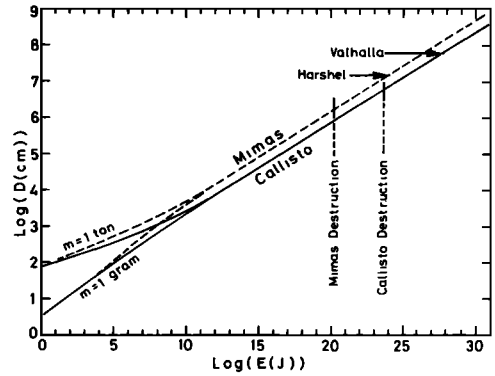

Fig. 9. Theoretical relation of crater diameter versus kinetic impact energy for Mimas and Callisto. The diameters fo the largest Craters on Mimas (Hershel) and Callisto (Valhalla), and the energies required for complete destruction of the both satellites are also shown.

$$D \propto g^{-1/4} \qquad (17)$$

rather than the experimentally determined relation [Gault and Wedekind, 1977; Schmidt and Holsapple, 1980],

$$D \propto g^{-1/6} \qquad (18)$$

because the latter relation is thought to be valid only for granular, noncohesive targets [Mizutani et al., 1983]. According to Figure 9, the impact kinetic energy which produced Valhalla, the largeest crater on Callisto, is estimated to be about 10^{27} joules. This corresponds to the specific energy of impact of 10^4 J/kg which is about three orders of magnitude larger than the specific energy for complete destruction of Callisto. The largest crater on Mimas is produced by an impact of about 10^{23} joules of kinetic energy which is also three orders of magnitude larger than the energy required for complete destruction of Mimas. Thus the giant impacts which produced large craters such as Valhalla on Callisto and Herschel (D = 150 km) on Mimas, have kinetic energies great enough to destroy these satellites. This may be due to the overestimation of the energy to produce a certain diameter of crater, or due to the underestimation of the energy to destroy the satellites. Even so, the present experimental data and our theoretical extrapolation suggest that these giant impacts must have fractured severely the whole satellites. Fragmentation of these satellites were probably prohibited by the fact that a larger energy is required to disperse the resulting fragments against the forces of self-gravities of the satellites [Lange and Ahrens, 1981]. Although we cannot see traces of these fractures associated with the giant impacts except concentric rings around the Valhalla, the impact energies should have given significant effects on the evolution of the satellites, via, e.g., shock heating, abrupt adiabatic pressure release due to fracturing, and subsequent plastic flow associated with crater landforms.

Acknowledgments. The authors thank M. A. Lange for his careful review which greatly improved the manuscript.

References

Anderson, G. D., The equation of state of ice and composite frozen soil material, interim technical report, project FGU-6392, contract DAAG 23-67-C-OD11, SRI Int., Menlo Park, Calif, 1967.

Butkovich, T. R., Mechanical properties of ice, Q. Colo. Sch. Mines., 54, 349-360, 1959.

Croft, S. K., Hypervelocity impact in icy media (abstract) in Lunar and Planetary Science XII, pp. 190-192, Lunar and Planetary Institute, Houston, 1981.

Croft, S. K., S. W. Kieffer, and T. J. Ahrens, Low-velocity impact craters in ice and ice-saturated sand with implications for martian crater count ages, J. Geophys. Res., 84, 8023-8032, 1979.

Curran, D. R., D. A. Shockey, L. Seamen, and M. Austin, Mechanics and models of cratering in earth media, in Impact and Explosion Cratering, edited by D. J. Roddy, R. O. Pepin and R. B. Merrill, Pergamon, New York, pp. 1057-1077, 1977.

Fujiwara, A., G. Kamimoto, and A. Tsukamoto, Destruction of basaltic bodies by high velocity impact, Icarus, 31, 277-288, 1977.

Fujiwara, A., G. Kamimoto, and A. Tsukamoto, Expected shape distribution of asteroids obtained from laboratory impact experiments, Nature, 272, 602-603, 1978.

Gault, D. E., Displaced mass, depth, diameter and effects of oblique trajectories for impact craters formed in dense crystalline rocks, The Moon, 6, 32-44, 1973.

Gault, D. E., and J. A. Wedekind, The destruction of tektites by micrometeoroid impact, J. Geophys. Res., 74, 6780-6794, 1969.

Gault, D. E., and J. A. Wedekind, Experimental hypervelocity impact into quartz sand -II. Effects of gravitational acceleration, in Impact and Explosion Cratering, edited by D. J. Roddy, R. O. Pepin and R. B. Merrill, pp. 1231-1244, Pergamon, New York, 1977.

Greenberg, R., J. F. Wacker, W. K. Hartmann, and C. R. Chapman, Planetesimals to planets: numerical simulation of collisional evolution, Icarus, 35, 1-26, 1978.

Hartmann, W. K., Planet formation: mechanism of early growth, Icarus, 33, 50-61, 1978.

Hobbs, P. V., Ice Physics, 837pp, Oxford Univ. Press, New York, 1974.

Hörz, F., Structural and mineralogical evaluation of an experimentally produced impact crater in granite, Contrib. Mineral. Petrol., 21, 365-377, 1969.

Hörz, F., J. B. Hartung, and D. E. Gault, Micrometeorite craters on lunar rock surfaces, J. Geophys. Res., 76, 5770-5798, 1971.

Kawakami, S., Impact cratering in quartz sand, ice and rocky materials, Master's thesis, Dept. Earth Sci., Nagoya Univ., Japan, 1982.

Kieffer, S. W., and C. H. Simonds, The role of volatiles and lithology in the impact cratering process, Rev. Geophys. Space Phys., 18, 143-181, 1980.

Lange, M. A. and T. J. Ahrens, Fragmentation of ice by low velocity impact, Proc. Lunar Planet. Sci. 12B, 1677-1687, 1981.

Lange, M. A. and T. J. Ahrens, Impact cratering in ice- and ice-silicate targets: an experimental assessment (abstract), in Lunar and Planetary Science XIII, pp. 415-416, Lunar and Planetary Institute, Houston, 1982a.

Lange, M. A., and T. J. Ahrens, Impact fragmentation of ice- and ice-silicate bodies (abstruct), in Lunar and Planetary Science XIII, pp. 417-418, Lunar and Planetary Institute, Houston, 1982b.

Lawn, B. R., and M. V. Swain, Microfracture beneath point indentation in brittle solids, J. Mater. Sci., 10, 113-122, 1975.

Lawn, B. R., and R. Wilshaw, Indentation fracture: principles and applications, J. Mater. Sci., 10, 1049-1081, 1975.

Masuda, K., I. Yamada and H. Mizutani, Compressive loading tests of ice and acoustic emissions associated with internal melting, Abstr. Seism. Soc. Japan, 127, 1982.

Matsui, T., Collisional evolution of mass distribution spectrum of planetesimals II, Proc. Lunar Planet. Sci. Conf. 10th, 1881-1895, 1979.

Mizutani, H., M. Kumazawa, M. Kato, T. Masuda, S. Kawakami, Y. Takagi, and K. Kani, A performance test of the low velocity shock gun with a noble sabot stopper, Proc. 14th ISAS Lunar and Planet. Symp., 267-277, 1981.

Mizutani, H. S. Kawakami, Y. Takagi, M. Kato, and M. Kumazawa, Cratering experiments in sands and a trial for general scaling law, J. Geophys. Res., 88, A835-A845, 1983.

Mizutani, H., and H. Spetzler, An unified theory of time-dependent behavior of brittle rocks, J. Geophys. Res., in press, 1983.

Schmidt, R. M., and K. A. Holsapple, Theory and experiments on centrifuge cratering, J. Geophys. Res., 85, 235-252, 1980.

Schumann, R. Jr., Principles of comminution, 1. Size distribution and surface calculations, Am. Inst. Min. Metall., Petrol. Eng. Tech. Publ., 1189, 1940.

Smith, B. A., L. A. Soderblom, T. V. Johnson, A. P. Ingersoll, S. A. Collins, E. M. Shoemaker, G. E. Hunt, H. Masursky, M. H. Carr, M. E. Davies, A. F. Cook II, J. Boyce, G. E. Danielson, T. Owen, C. Sagan, R. F. Beek, J. Veverka, V. E. Suomi (Voyager Imaging Team), The Jupiter system through the eyes of Voyager 1, Science, 204, 951-972, 1979.

Smith B. A., L. Soderblom, R. Beebe, J. Boyce, G. Briggs, A. Bunker, S. A. Collins, C. J. Hansen, T. V. Johnson, J. L. Mitchell, R. J. Terrile, M. Carr, A. F. Cook II, J. Cuzzi, J. B. Pollack, G. E. Danielson, A. Ingersoll, M. E. Davies, G. E. Hunt, H. Masursky, E. Shoemaker, D. Morrison, T. Owen, C. Sagan, J. Veverka, R. Strom, V. E. Suomi (Voyager Imaging Team), Encounter with Saturn:Voyager 1 imaging science results, Science, 212, 159-190, 1981.

Summers, J. L., and A. C. Charters, High-speed impact of metal projectiles in targets of various materials, Proc. Symp. Hypervelocity Impact, 3rd, pp. 101-113, Armour Res. Foundation, Chicago, 1959.

Takeuchi, H., and H. Mizutani, Relation between earthquake occurrence and brittle fracture (in Japanese), Kagaku, 38, 622-624, 1968.

(Received May 25, 1982;
revised October 7, 1982;
accepted November 9, 1982)